The 9th European Congress on Computational Methods in Applied Sciences and Engineering
ECCOMAS Congress 2024
3–7 June 2024, Lisboa, Portugal

HARMONIC BEHAVIOR OF FUNCTIONALLY GRADED I-SHAPE BEAMS USING THE THERMOELASTIC MODEL

ANDRÉ CARVALHO[1]

[1] CIMOSM, ISEL – Centro de Investigação em Modelação e Optimização de Sistemas Multifuncionais, Instituto Politécnico de Lisboa, R. Concelheiro Emídio Navarro 1, 1959-007, Lisboa, Portugal, andre.carvalho@isel.pt, https://cimosm.isel.pt

Key words: Finite element method, Thermoelastic model, Harmonic analysis, Functionally Graded Materials, Damping

Summary. Functionally graded materials are renowned for minimizing abrupt stress transitions typical of laminated composites. They are highly suitable for operation in adverse high-temperature environments and can act as thermal barriers, especially when considering a proper selection of constituent materials. While these materials have been the subject of intense research by the scientific community, existing studies have predominantly focused on rectangular cross-section beams or plates. Beams with different cross-section profiles can also benefit from the continuous smooth material transition of functionally graded materials. Therefore, this study explores the influence of functionally graded materials on the harmonic behavior of symmetrical I-beams, with emphasis on the damping behavior. The investigation involves a parametric analysis using the thermoelastic model. The beams undergo harmonic loading variations, with subsequent study of the resulting spectra and damping behavior. As anticipated, the material mixtures and shapes influence harmonic behaviors and damping profiles.

1 INTRODUCTION

Thermoelastic damping is inherent in all structures and constitutes a source of structural damping [7, 6]. The thermoelastic model is derived from fundamental principles, fully integrating the elastic wave equation with the heat equation. Although the origins of this model date back to the 1950s [3, 5], its complexity necessitated the development of modern computational resources to enable thorough analysis [19, 4, 22, 14, 5, 6]. The damping mechanism in thermoelasticity comes from the irreversible Entropy generation due to deformation created by internal heat fluxes. Energy loss due to the thermoelastic effect is more pronounced in smaller or larger structures at low frequencies [6, 12, 10, 9]. In microscale mechanisms, the impact of temperature on vibration is significant and cannot be disregarded [23, 24], leading to a need for a comprehensive understanding of this effect, which is crucial for the engineering of optimized solutions. Depending on the type of mechanism, damping may be undesirable, as in microresonators [23, 24, 21], or desirable, as in microscale damper mechanisms [13, 8, 11].

The engineering of tailored damping mechanisms can also use more advanced materials. Functionally Graded Materials (FGM) are composite materials characterized by a continuous variation in composition without distinct phase boundaries [16, 15, 18]. This continuous gradation enables the engineering of single-component structures with varying mechanical properties

across their geometry. FGMs also exhibit enhanced thermal properties and improved fracture resistance [16]. Applying FGMs to microstructures introduces an additional level of customization of mechanical properties [1, 20].

Since I-beams are standard structural members, a thorough understanding of the dynamic behavior of these elements, particularly regarding damping, is essential for designing structures capable of withstanding dynamic loads. Numerous studies have explored thermoelasticity in beams or plates, both at regular and micro/nano scales, predominantly focusing on elements with rectangular cross-sections [5, 9, 12, 10, 23, 26, 17, 19, 4, 22]. An analysis of thermoelastic effects in steel I-beams can be found in [6]. Therefore, the primary objective of this study is to investigate thermoelastic damping and its dependence on frequency, geometry, and material composition.

The case studies presented in this work examine beams subjected to bending loads, employing Finite Element Analysis (FEA) based on solid elements rather than conventional beam or plate elements [22, 4, 5, 23, 24]. Solid elements are computationally more demanding due to the requirement for finer meshes to capture bending phenomena accurately. However, they offer greater versatility and insight into local phenomena, such as detailed temperature variation across the thickness [6]. Additionally, when applied to FGMs, solid elements provide more precise control over material distribution [16].

This article is structured into four sections: Introduction, Materials and Methods, Results and Discussion, and Conclusions. The Materials and Methods section elaborates on the formulation of the thermoelastic model and the 3D quadratic hexahedral solid elements. The Results and Discussion section covers the mesh generation process, convergence studies, and simulation results. The Conclusions section provides a summary of the study's findings.

2 MATERIALS AND METHODS

2.1 The Thermoelastic Model

The thermoelastic model results from the full coupling of the elastic wave equation with the heat equation and is given by (1):

$$\begin{cases} \rho\ddot{\mathbf{u}} - \mu\nabla^2\mathbf{u} - (\lambda+\mu)\nabla(\nabla\cdot\mathbf{u}) + \gamma\nabla\theta = f \\ \rho C_p\dot{\theta} - \kappa\nabla^2\theta + \gamma T_0(\nabla\cdot\dot{\mathbf{u}}) = q, \end{cases} \tag{1}$$

where $\mathbf{u}$ is the displacement vector ($\mathbf{u} = [u_x, u_y, u_z]^T$), θ is the temperature variation, f is the body load and q is the body heat flux. All function quantities are functions of the Euclidean coordinates and time. The constants in the model are the material properties: density (ρ), Lamé constants (μ and λ), specific heat capacity (C_p), and thermal conductivity (κ).

Equation (1) is linearized around the base temperature T_0, and, as such, it is only valid for small deformations and small temperature variations: $\frac{\theta}{T_0} \ll 1$. Finally, the coefficient γ is the coupling term and is given by:

$$\gamma = (3\lambda + 2\mu)\alpha, \tag{2}$$

where α is the linear thermal expansion coefficient.

2.2 Finite Element model

The thermoelastic model was implemented on an in-house Finite Element Analysis software in 2D quadrilateral and 3D hexahedral solid elements (linear and quadratic), [6]. The software was written in C++ and Intel® Math Kernel Library performs the linear algebra routines.

For this study, a solid standard 27 nodes quadratic hexahedral 3D element was defined according to the Fig. 1.

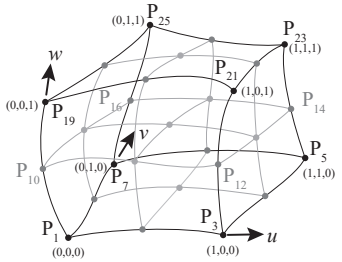

Figure 1: Twenty seven node 3D quadratic solid element.

The full discretized version of (1) is given by (3)

$$\boldsymbol{\mathcal{M}} \begin{bmatrix} \ddot{\mathbf{u}}_x \\ \ddot{\mathbf{u}}_y \\ \ddot{\mathbf{u}}_z \\ \ddot{\boldsymbol{\theta}} \end{bmatrix} + \boldsymbol{\mathcal{C}} \begin{bmatrix} \dot{\mathbf{u}}_x \\ \dot{\mathbf{u}}_y \\ \dot{\mathbf{u}}_z \\ \dot{\boldsymbol{\theta}} \end{bmatrix} + \boldsymbol{\mathcal{K}} \begin{bmatrix} \mathbf{u}_x \\ \mathbf{u}_y \\ \mathbf{u}_z \\ \boldsymbol{\theta} \end{bmatrix} = \begin{bmatrix} \mathbf{Mf}_x \\ \mathbf{Mf}_y \\ \mathbf{Mf}_z \\ \mathbf{Mq} \end{bmatrix} \tag{3}$$

where u_x, u_y and u_z are the displacements in the x, y and z directions, respectively, $\boldsymbol{\mathcal{M}}$, $\boldsymbol{\mathcal{C}}$ and $\boldsymbol{\mathcal{K}}$, are the mass, velocity[1] and stiffness matrices. For more details on the matrices, please refer to [6].

The damping coefficient can be extracted from the work made by a load (or from the dissipated energy) using the maximum elastic potential energy:

$$\eta(\omega) = \frac{W_{S_{\text{cycle}}}}{\pi k \Re(X)^2}, \tag{4}$$

where k is the stiffness of the spring, and X is the complex amplitude of the displacement, and $W_{S_{\text{cycle}}}$ is the dissipated work, [6]. The denominator of (4) is the maximum potential energy in a cycle.

2.3 Geometries and materials

Functionally graded materials change material properties by progressively mixing two (or more) materials in a given direction. For this study, the function that provides volume fraction is based on the function shown in [16]. The function in (5) is an exponential law-based function

[1]The term damping matrix should be avoided because the damping in the thermoelastic model is not completely contained in this matrix.

that is flexible to ensure a more controlled material distribution.

$$\begin{cases} V_A & 0 \leq \frac{z}{H} < zmin \\ \frac{(V_A - Q_1)\left(\cosh\left(Q_{2_A}\left(\frac{z}{H} - zcut_A\right)\right) - 1\right)}{\cosh(Q_{2_A}(zmin - zcut_A)) - 1} + Q_1 & zmin \leq \frac{z}{H} < zcut_A \\ Q_1 & zcut_A \leq \frac{z}{H} < zcut_B \\ \frac{(V_B - Q_1)\left(\cosh\left(Q_{2_B}\left(\frac{z}{H} - zcut_B\right)\right) - 1\right)}{\cosh(Q_{2_B}(zmax - zcut_B)) - 1} + Q_1 & zcut_B \leq \frac{z}{H} \leq zmax \\ V_B & zmax < \frac{z}{H} \leq 1 \end{cases}, \tag{5}$$

where V_A and V_B are the fractions of the material at the end-points, $zmin$ and $zmax$ are the size of the saturation region at the end-points, Q_1 is the minimum fraction of the material at the center, $zcut_A$ and $zcut_B$ control the position and length of the middle plateau, and Q_{2_A} and Q_{2_B} control the slope of the exponential for the left and right sides.

In this study, the parameters used result in a symmetrical material distribution with a constant material distribution in the flanges of the I-beams. Also, to reduce the numerical complexity of the model, the material distribution was discretized according to the number of elements heigh-wise (keeping the material constant at the flanges of the I-beams), Fig. 2. The parameters are shown in Table 1.

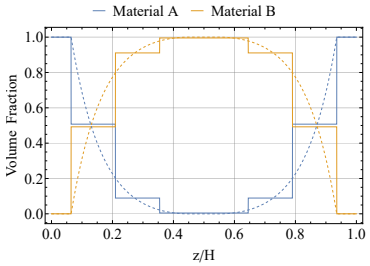

Figure 2: Volume fraction function used to control the material mixing in the z direction and its discretized version.

Q_1	0
Q_{2_A}	10
Q_{2_B}	10
$zmin$	6.44%
$zmax$	93.56%
$zcut_A$	45%
$zcut_B$	55%
V_A	1
V_B	1

Table 1: Parameters for the volume fraction function.

The materials used in the study were a standard generic steel and Alumina (Al_2O_3). The mechanical and thermal properties of the materials can be seen in Table 2. All properties are given for a base temperature of 293.15K

Property	**Unit**	**Steel**	**Alumina** (Al_2O_3)
Young Modulus	GPa	200	380
Poisson coefficient	-	0.3	0.3
Density	kg/m^3	7800	3800
Thermal expansion coefficient	K^{-1}	12×10^{-6}	8×10^{-6}
Thermal conductivity	$W/(m \cdot K)$	45	31.5*
Specific heat capacity	$J/(kg \cdot K)$	470	703*

Table 2: Material properties (properties of the Alumina marked with an "*" mean the average value of the range was used).

In this work, two geometries are studied: a symmetrical ASTM A6 wide flange I-beam (W150x100x24.0, Fig. 3 and Table 3) and a square 160mm thick beam.

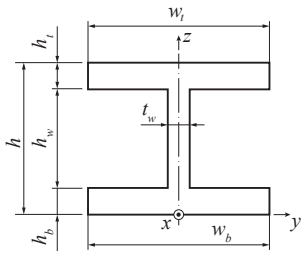

Figure 3: I-beam dimensions

Dimension	**Value** (mm)
t_w	6.6
h_w	139.4
w_b	102
h_b	10.3
w_t	102
h_t	10.3
h	160

Table 3: Dimensions of the section of a W150x100x24.0 wide flange beam.

The aspect ratio (height vs. length) of all beams is 20 (corresponding to a 3.2m beam for 160mm height). Different beams with different uniform scales were also used to study how thermoelastic damping changes with size.

3 RESULTS AND DISCUSSION

3.1 Mesh convergence

The software and models used in this study were validated against other models and works. Full details on the validation studies can be consulted in [16] and [6].

Only two geometries were used in this study: the I-beam and the square-section beam, and, as such, only two meshes were used. Since by scaling uniformly the beams, the relations between the dimensions do not change, the same number and distribution of elements can be used. To determine the mesh parameters, a mesh convergence study was done for both meshes. Since this article uses only harmonic simulations, the convergence of the first two natural vertical bending frequencies was chosen as the convergence criterion. The mesh convergence for the I-beam can be seen graphically in Fig. 4a. The selected mesh was the second last, with 160 elements across the length. A similar process was followed for the rectangular-section beam, reaching a stabilized mesh of 160 by 5 by 9 elements (length/width/height).

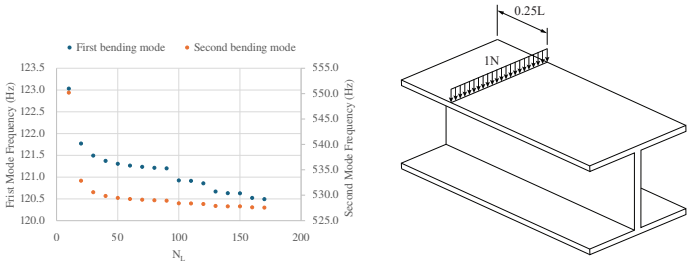

(a) (b)

Figure 4: (a) Convergence of the first two natural frequencies for the W150x100x24.0 beam (1.6m length), (b) Amplitude and position of the applied distributed load.

3.2 Case studies

For this work, 24 case studies were used. All case studies use beams with a 20:1 ratio to the total height (20H), and all cases use a harmonic 1N amplitude distributed load applied at a quarter length of the beam, Fig. 4b.

3.3 Simulation results - square beam

Making a frequency sweep from 0 to 200rad/s and using (4) (more specifically, the version for the finite element model in [6]), the evolution of the equivalent damping coefficient with frequency for the rectangular beams with only a single material can be seen in Fig. 5

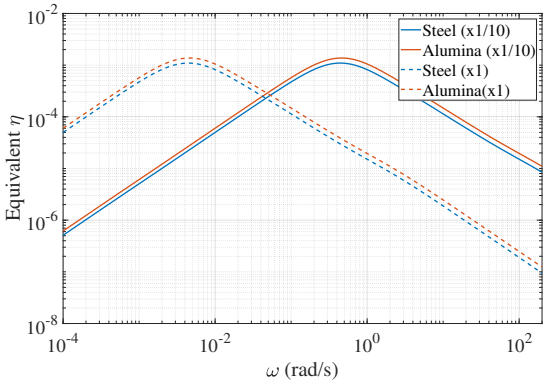

Figure 5: Damping vs. frequency for Steel and Alumina square-section beams (full scale and 1/10).

Fig. 5 shows the typical behavior of the thermoelastic damping for rectangular beams, with a maximum value and decreasing to zero as the frequency increases (and decreases because it is 0 at a frequency of 0), has reported by [25, 14, 2, 7]. The shift in the frequency of the maximum point between the two scales is also in line with expectations, where the frequency of the maximum increases with the reduction in the beam size. Because the beams were scaled uniformly, the relation between the maxima is the squared scale. Regarding the two materials, it can be seen that Alumina has an overall higher damping than the steel beams. To better compare different beams, Zener in [25] proposed a frequency scaling time constant that removes the effect of the geometry of the beam, (3.3):

$$\tau_Z = \frac{\rho C_P t^2}{\pi^2 \kappa}, \tag{6}$$

where t is the thickness of the beam and τ_Z is Zener's time constant or the "characteristic relaxation time" [25].

Applying the scaling term to the beams, the effect of the geometry in the frequency is removed, with the resulting curves depending only on the material properties, Fig. 6a.

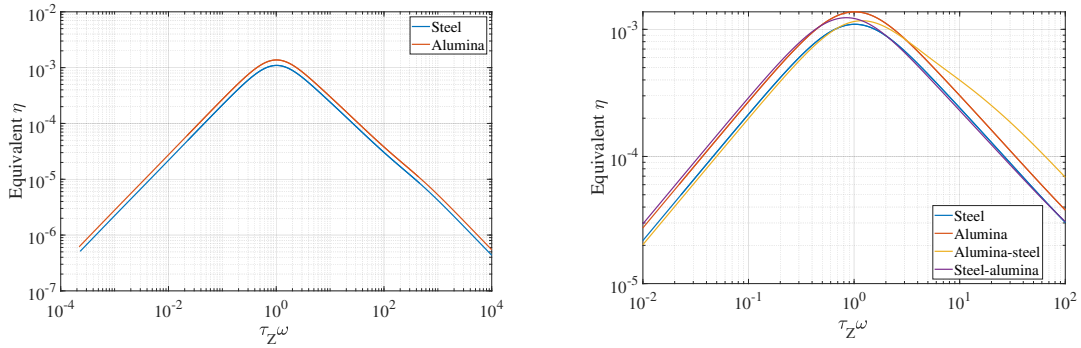

(a) (b)

Figure 6: Damping vs. frequency for: (a) Steel and Alumina square-section beams with scaled frequencies, (b) square-section beams with unmodified scaled frequencies.

Adding the results for the FGM beams (both Steel-alumina and Alumina-steel beams), it can be seen that even by applying the frequency scaling with (3.3), the damping curves do not align with the others, Fig. 6b. The average properties of the FGM beams were obtained by computing the highest time constant for the heat equation, and since the first time constant for prismatic bodies is given by (7a), Zener's time constant can be obtained by the relation in (7b).

$$\tau_1 = \frac{\rho C_P L^2}{\pi^2 \kappa}, \tag{7a}$$

$$\tau_Z = \tau_1 \left(\frac{t}{L}\right)^2 \tag{7b}$$

where τ_1 is the highest time constant of the heat equation (the inverse of the first pole) and L is the length of the beam.

This happens because Zener's time constant is the inverse of the first pole of the differential equation in (8):

$$\frac{\kappa}{\rho C_P}\nabla^2 U + \tau_Z^{-1} U = 0, \tag{8}$$

where U is the "orthogonal thermodynamic potential" [25]. Since the material distribution is not constant, the first pole of (8) will be different than .

Using the first time constants of the heat equation of both FMG distributions, an equivalent beam thickness can be found to align all damping curves, and (7b) can be adapted into (9):

$$\tau_Z = \tau_1 \left(\frac{at}{L}\right)^2, \tag{9}$$

where a is a positive scaling term, which for the square-section beams is given in Table 4. Applying (9) with the values in Table 4, Fig. 6b becomes Fig. 7a.

At the maximum damping point, the FGM distribution with the highest damping damping value is the one with alumina at the center. This happens because the irreversible entropy generation is higher where the heat flux is higher (in absolute). Plotting the heat flux for all

Material A	Material B	Scaling term a
Steel	Steel	1
Alumina	Alumina	1
Alumina	Steel	0.916
Steel	Alumina	1.086

Table 4: Case studies used in the work.

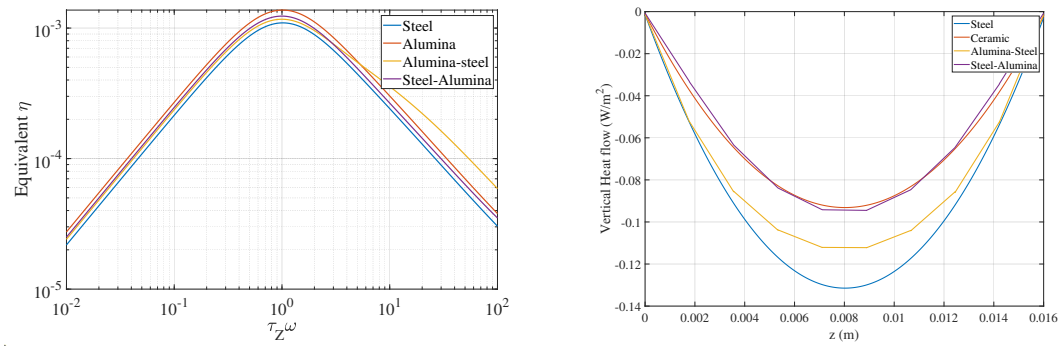

(a) (b)

Figure 7: (a) Damping vs. frequency for square-section beams with modified scaled frequencies, (b) Vertical heat flux (zz axis direction) across the beam thickness.

beams about the beam thickness, Fig. 7b shows that the heat flux has a behavior similar in shape to the shear stress distribution. Although it is not visible, the maximum values of the curves in Fig. 7b are not in the middle of the beam. Because they were taken at the point where the load was applied, there is a small compression of the thickness, and consequently, the temperature is slightly biased to the positive variation. The discontinuity in the heat flux can also be seen every time there is a variation in the material composition on the FGM distributions.

3.4 Simulation results - I-beam

Moving to the I-beams simulations, the tests show a new type of behavior for the damping. In the simulations for the I-beams made from steel and alumina, the damping behavior with frequency is displayed on Fig. 8a. The deformated beam (with a high scaling factor) can be seen in Fig. 8b.

The first observation is that instead of the familiar shape of the thermoelastic damping curve for I-beams, the damping curve now has two maxima. The reason for the second maximum will be discussed later.

Since the beam section is no longer rectangular, the solution to (8) is different. Using the same method as before, the scaling term a in (9) can be found for the W150 I-beam:

$$\tau_Z = \tau_1 \left(\frac{0.11t}{L} \right)^2, \tag{10}$$

where $a = 0.11$. This means that the maximum damping frequency of a W150 I-beam is equivalent to a rectangular beam with 11% thickness.

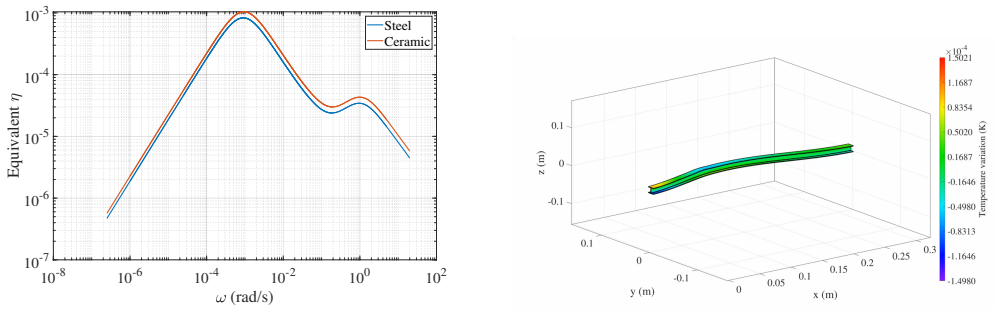

(a) (b)

Figure 8: (a) Damping vs. frequency for I-beams made of steel and alumina, (b) W150 I-beam at the maximum deformation.

Adding the results for the simulations with the FGM distributions and scaling the frequencies, the resulting plot can be seen in Fig. 9a. As expected, the solution to (8) is also different due to

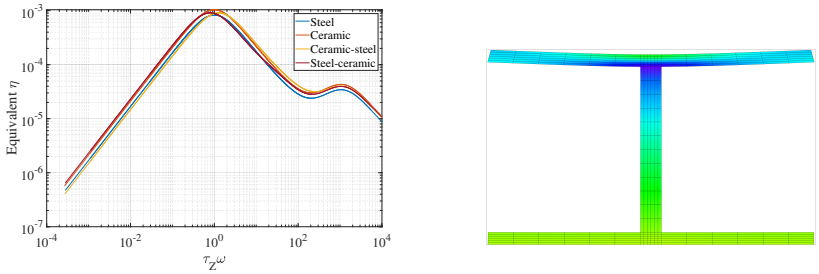

(a) (b)

Figure 9: (a) Damping vs. frequency for I-beams with modified scaled frequencies, (b) Cross-section of the W150 I-beam at maximum deformation showing the local flang deformation (darker regions denote negative temperature variations, and the brighter regions denote positive temperature variations).

the material distribution being different across the thickness of the beam. However, this time, there is a slight difference. While the first maxima are misaligned, the second is not, and because of this, it is impossible to replicate Fig. 7a for I-beams. This happens due to the nature of the second maxima.

As stated above, the thermoelastic model predicts that the larger the internal heat fluxes, the larger the damping coefficient. When studying a square-section beam under bending, the heat flux is vertical. However, this is different for an I-beam. Making a plot of the I-beam cross-section at the load application point, it can be seen that there is a local deformation of the flange, Fig. 9b. This local deformation generates a horizontal heat flux that is simultaneous with the main vertical flux and is responsible for the second maxima. Since the material distribution for the FGM I-beams is only vertical and the flanges have a constant distribution of material, the second maxima are aligned in Fig. 9a, while the first is not.

When comparing the influence of the cross-section more directly, Fig. 10, it can be seen

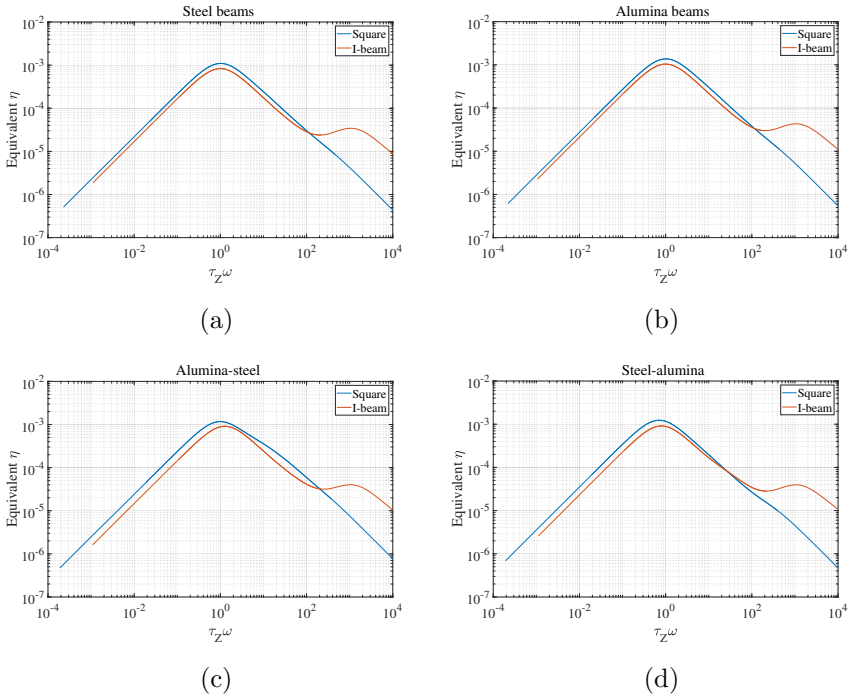

Figure 10: Damping vs. frequency comparing different cross-sections with the same material distribution: (a) Steel, (b) Alumina, (c) Alumina-steel, and (d) Steel-alumina.

that the square cross-section has a higher damping coefficient for lower frequencies, and the I-beam has higher damping in higher frequencies; the overall behavior is similar. The damping coefficient values are not significantly different. When focusing on the FGM beams (Fig. 10c and Fig. 10d), because the Steel-alumina has a higher level of alumina closer to the neutral line, the overall damping is higher (much like the case of the square beams, the behavior of the heat flux in I-beam is analogous to the shear stress).

4 CONCLUSIONS

This research aimed to study the damping behavior of I-beams composed of functionally graded materials (FGMs) due to the inherent thermoelastic effect. The results from simulations using harmonic Finite Element Analysis reveal the following:

- Alumina exhibits a higher damping coefficient (or Q-factor, Q^{-1}) than steel. When comparing the damping of an FGM distribution between steel and alumina, the damping value falls in between.
- Damping is more influenced by the material closest to the neutral axis. For an FGM beam, damping can be increased by incorporating a higher percentage of steel in the flanges (maximizing resistance to bending deformations) and a higher rate of alumina in the web.
- For I-beam cross-sections, the damping curve exhibits a second maximum at higher fre-

quencies. This second maximum is caused by local bending of the flanges due to the applied load.

REFERENCES

[1] Behrokh Abbasnejad and Ghader Rezazadeh. Mechanical behavior of a fgm micro-beam subjected to a nonlinear electrostatic pressure. *International Journal of Mechanics and Materials in Design*, 8(4):381–392, 2012.

[2] Holt Ashley. On passive damping mechanisms in large space structures. *Journal of Spacecraft and Rockets*, 21(5):448–455, 1984.

[3] M. A. Biot. Thermoelasticity and irreversible thermodynamics. *Journal of Applied Physics*, 27(3):240–253, 1956.

[4] J.E. Bishop and V.K. Kinra. Thermoelastic damping of a laminated beam in flexure and extension. *Journal of Reinforced Plastics and Composites*, 12(2):210–226, 1993.

[5] B. A. Boley and A. D. Barber. Dynamic response of beams and plates to rapid heating. *J. Appl. Mech.*, 24(3):413–416, 1957.

[6] André Carvalho. Study of damping of bare and encased steel i-beams using the thermoelastic model. *Buildings*, 13(12), 2023.

[7] André Carvalho. Study of the influence of convection boundary condition on the damping factor in a thermoelastic beam using solid elements. In *Proceedings of 6th International Conference on Numerical and Symbolic Computation*, pages 151–168, 2023.

[8] A Fichera, A Pagano, and R Volpe. Microscale damper prototype: A preliminary study on suppressing air flow oscillations within microchannels. *Journal of Physics: Conference Series*, 2685(1):012022, jan 2024.

[9] Sayantan Guha and Abhishek Kumar Singh. Frequency shifts and thermoelastic damping in different types of nano-/micro-scale beams with sandiness and voids under three thermoelasticity theories. *Journal of Sound and Vibration*, 510:116301, 2021.

[10] F.L. Guo, G.Q. Wang, and G.A. Rogerson. Analysis of thermoelastic damping in micro- and nanomechanical resonators based on dual-phase-lagging generalized thermoelasticity theory. *International Journal of Engineering Science*, 60:59–65, 2012.

[11] S. S. Iyer, R. Vedad-Ghavami, H. Lee, M. Liger, H. P. Kavehpour, and R. N. Candler. Nonlinear damping for vibration isolation of microsystems using shear thickening fluid. *Applied Physics Letters*, 102(25):251902, 06 2013.

[12] Ehsan Kazemnia Kakhki, Seyed Mahmoud Hosseini, and Masoud Tahani. An analytical solution for thermoelastic damping in a micro-beam based on generalized theory of thermoelasticity and modified couple stress theory. *Applied Mathematical Modelling*, 40(4):3164–3174, 2016.

[13] Catherine A. Kerrigan, Ken K. Ho, K. P. Mohanchandra, and Gregory P. Carman. Microscale damping using thin film active materials. In Yuji Matsuzaki, Mehdi Ahmadian, and Donald J. Leo, editors, *Active and Passive Smart Structures and Integrated Systems 2007*, volume 6525, page 65250V. International Society for Optics and Photonics, SPIE, 2007.

[14] V. K. Kinra and K. B. Milligan. A Second-Law Analysis of Thermoelastic Damping. *Journal of Applied Mechanics*, 61(1):71–76, 03 1994.

[15] M. Koizumi. Fgm activities in japan. *Composites Part B: Engineering*, 28(1):1–4, 1997. Use of Composites Multi-Phased and Functionally Graded Materials.

[16] M.A.R. Loja, André Carvalho, and Ines C.J. Barbosa. A study on the static behavior of functionally graded i-shaped beams. *AIMS Materials Science*, 11(1):28–57, 2024.

[17] R. Resmi, V. Suresh Babu, and M.R. Baiju. Thermoelastic damping limited quality factor enhancement and energy dissipation analysis of rectangular plate resonators using nonclassical elasticity theory. *Advances in Materials Science and Engineering*, 2022, 2022. Cited by: 0; All Open Access, Gold Open Access.

[18] Atteshamuddin S. Sayyad and Yuwaraj M. Ghugal. Modeling and analysis of functionally graded sandwich beams: a review. *Mechanics of Advanced Materials and Structures*, 26(21):1776–1795, 2019.

[19] Enrico Serra and Michele Bonaldi. A finite element formulation for thermoelastic damping analysis. *International Journal for Numerical Methods in Engineering*, 78(6):671–691, 2009.

[20] Naser Sharafkhani, Ghader Rezazadeh, and Rasool Shabani. Study of mechanical behavior of circular fgm micro-plates under nonlinear electrostatic and mechanical shock loadings. *Acta Mechanica*, 223(3):579–591, 2012.

[21] J.N. Sharma and R. Sharma. Damping in micro-scale generalized thermoelastic circular plate resonators. *Ultrasonics*, 51(3):352–358, 2011.

[22] Alexandros G Solomou, Theodoros T Machairas, and Dimitris A Saravanos. A coupled thermomechanical beam finite element for the simulation of shape memory alloy actuators. *Journal of Intelligent Material Systems and Structures*, 25(7):890–907, 2014.

[23] Yuxin Sun, Daining Fang, and Ai Kah Soh. Thermoelastic damping in micro-beam resonators. *International Journal of Solids and Structures*, 43(10):3213–3229, 2006.

[24] Yuxin Sun and Masumi Saka. Thermoelastic damping in micro-scale circular plate resonators. *Journal of Sound and Vibration*, 329(3):328–337, 2010.

[25] Clarence Zener. Internal friction in solids. i. theory of internal friction in reeds. *Phys. Rev.*, 52:230–235, Aug 1937.

[26] Wanli Zuo, Pu Li, Jianke Du, and Zion Tsz Ho Tse. Thermoelastic damping in anisotropic piezoelectric microbeam resonators. *International Journal of Heat and Mass Transfer*, 199:123493, 2022.